Modeling dispersive coupling and losses of localized optical and mechanical modes in optomechanical crystals

Matt Eichenfield*, Jasper Chan*, Amir H. Safavi-Naeini, Kerry J. Vahala, and Oskar Painter

Thomas J. Watson, Sr, Laboratory of Applied Physics, California Institute of Technology, Pasadena, California 91125, USA

opainter@caltech.edu

Abstract: Periodically structured materials can sustain both optical and mechanical excitations which are tailored by the geometry. Here we analyze the properties of dispersively coupled planar photonic and phononic crystals: optomechanical crystals. In particular, the properties of co-resonant optical and mechanical cavities in quasi-1D (patterned nanobeam) and quasi-2D (patterned membrane) geometries are studied. It is shown that the mechanical Q and optomechanical coupling in these structures can vary by many orders of magnitude with modest changes in geometry. An intuitive picture is developed based upon a perturbation theory for shifting material boundaries that allows the optomechanical properties to be designed and optimized. Several designs are presented with mechanical frequency $\sim$ 1-10 GHz, optical Q-factor $Q_o > 10^7$, motional masses $m_{\rm eff} \approx 100$ femtograms, optomechanical coupling length $L_{\rm OM} < 5$ μm, and clampinig losses that are exponentially suppressed with increasing number of phononic crystal periods (radiation-limited mechanical Q-factor $Q_m > 10^7$ for total device size less than 30 μm).

OCIS codes: (230.5298) Photonic crystals; (230.4685) Optical microelectromechanical devices; (230.5750) Resonators; (350.4855) Optical tweezers or optical manipulation.

References and links

1. M. Maldovan and E. L. Thomas, "Simultaneous localization of photons and phonons in two-dimensional periodic structures," Appl. Phys. Lett. **88**(25), 251907 (pages 3) (2006).
2. M. Eichenfield, J. Chan, R. Camacho, K. J. Vahala, and O. Painter, "Optomechanical Crystals," Nature, DOI:10.1038/nature08524 (2009).
3. T. J. Kippenberg and K. J. Vahala, "Cavity Optomechanics," Opt. Express **15**(25), 172–205 (2007).
4. T. J. Kippenberg and K. J. Vahala, "Cavity Optomechanics: Back-Action at the Mesoscale," Science **321**(5893), 1172–1176 (2008).
5. I. Favero and K. Karrai, "Optomechanics of deformable optical cavities," Nature Physics **3**(4), 201–205 (2009).
6. M. Trigo, A. Bruchhausen, A. Fainstein, B. Jusserand, and V. Thierry-Mieg, "Confinement of Acoustical Vibrations in a Semiconductor Planar Phonon Cavity," Phys. Rev. Lett. **89**(22), 227,402 (2002).
7. M. S. Kang, A. Nazarkin, A. Brenn, and P. S. J. Russell, "Tightly trapped acoustic phonons in photonic crystal fibres as highly nonlinear artificial Raman oscillators," Nat Phys **5**(4), 276–280 (2009).
8. J. S. Foresi, P. R. Villeneuve, J. Ferrera, E. R. Thoen, G. Steinmeyer, S. Fan, J. D. Joannopoulos, L. C. Kimerling, H. I. Smith, and E. P. Ippen, "Photonic-Bandgap microcavities in optical waveguides," Nature **390**, 143–145 (1997).
9. O. Painter, R. K. Lee, A. Yariv, A. Scherer, J. D. O'Brien, P. D. Dapkus, and I. Kim, "Two-dimensional photonic band-gap defect mode laser," Science **284**, 1819–1824 (1999).

#115150 - $15.00 USD Received 3 Aug 2009; revised 14 Sep 2009; accepted 22 Sep 2009; published 20 Oct 2009

10. J. Chan, M. Eichenfield, R. Camacho, and O. Painter, "Optical and mechanical design of a "zipper" photonic crystal optomechanical cavity," Opt. Express **17**(5), 3802–3817 (2009).
11. M. Pinard and Y. Hadjar and A. Heidmann, "Effective mass in quantum effects of radiation pressure," Eur. Phys. J. D **7**, 107–116 (1999).
12. T. Carmon and K. J. Vahala, "Optomechanical Modal Spectroscopy of Optoexcited Vibrations of a Micron-Scale on-Chip Sphere at Greater than 1 GHz," Phys. Rev. Lett. **98**(123901) (2007).
13. M. Tomes and T. Carmon, "Photonic Micro-Electromechanical Systems Vibrating at X-band (11-GHz) Rates," Phys. Rev. Lett. **102**(11), 113601 (pages 4) (2009).
14. O. Arcizet, P. F. Cohadon, T. Briant, M. Pinard, A. Heidmann, J. M. Mackowski, C. Michel, L. Pinard, O. Francais, and L. Rousseau, "High-Sensitivity Optical Monitoring of a Micromechanical Resonator with a Quantum-Limited Optomechanical Sensor," Phys. Rev. Lett. **97**, 133601 (2006).
15. I. Tittonen, G. Breitenbach, T. Kalkbrenner, T. Müller, R. Conradt, S. Schiller, E. Steinsland, N. Blanc, and N. F. de Rooij, "Interferometric measurements of the position of a macroscopic body: Towards observation of quantum limits," Phys. Rev. A **59**(2), 1038–1044 (1999).
16. V. B. Braginskiĭ, F. Y. Khalili, and K. S. Thorne, *Quantum measurement* (Cambridge University Press, Cambridge, 1992).
17. V. Braginsky and S. P. Vyachanin, "Low quantum noise tranquilizer for Fabry Perot interferometer," Phys. Lett. A **293**(5-6), 228–234 (2002).
18. S. Gigan, H. R. Böhm, M. Paternostro, F. Blaser, G. Langer, J. B. Hertzberg, K. C. Schwab, D. Bäuerle, M. Aspelmeyer, and A. Zeilinger, "Self-cooling of a micromirror by radiation pressure," Nature **444**, 67–70 (2006).
19. O. Arcizet, P.-F. Cohadon, T. Briant, M. Pinard, and A. Heidmann, "Radiation-pressure cooling and optomechanical instability of a micromirror," Nature **444**, 71–73 (2006).
20. D. Kleckner and D. Bouwmeester, "Sub-kelvin optical cooling of a micromechanical resonator," Nature **444**, 75–78 (2006).
21. A. Schliesser, P. Del'Haye, N. Nooshi, K. J. Vahala, and T. J. Kippenberg, "Radiation Pressure Cooling of a Micromechanical Oscillator Using Dynamical Backaction," Phys. Rev. Lett. **97**, 243905 (2006).
22. V. B. Braginsky, S. E. Strigin, and S. P. Vyatchanin, "Parametric oscillatory instability in Fabry-Perot interferometer," Phys. Lett. A **287**(5-6), 331 – 338 (2001).
23. T. J. Kippenberg, H. Rokhsari, T. Carmon, A. Scherer, and K. J. Vahala, "Analysis of Radiation-Pressure Induced Mechanical Oscillation of an Optical Microcavity," Phys. Rev. Lett. **95**(3), 033901 (2005).
24. K. J. Vahala, "Back-action limit of linewidth in an optomechanical oscillator," Phys. Rev. A (Atomic, Molecular, and Optical Physics) **78**(2), 023832 (pages 4) (2008).
25. Y.-C. Wen, L.-C. Chou, H.-H. Lin, V. Gusev, K.-H. Lin, and C.-K. Sun, "Efficient generation of coherent acoustic phonons in (111) InGaAs/GaAs multiple quantum wells through piezoelectric effects," Appl. Phys. Lett. **90**(17), 172102 (pages 3) (2007).
26. N. D. Lanzillotti-Kimura, A. Fainstein, A. Huynh, B. Perrin, B. Jusserand, A. Miard, and A. Lemaitre, "Coherent Generation of Acoustic Phonons in an Optical Microcavity," Phys. Rev. Lett. **99**(21), 217405 (pages 4) (2007).
27. R. H. O. III and I. El-Kady, "Microfabricated phononic crystal devices and applications," Measurement Scie. Technol. **20**(1), 012,002 (13pp) (2009).
28. R. H. O. III, I. F. El-Kady, M. F. Su, M. R. Tuck, and J. G. Fleming, "Microfabricated VHF acoustic crystals and waveguides," Sensors Act. A: Physical **145-146**, 87 – 93 (2008).
29. J. V. Sánchez-Pérez, D. Caballero, R. Mártinez-Sala, C. Rubio, J. Sánchez-Dehesa, F. Meseguer, J. Llinares, and F. Gálvez, "Sound Attenuation by a Two-Dimensional Array of Rigid Cylinders," Phys. Rev. Lett. **80**(24), 5325–5328 (1998).
30. W. M. Robertson and J. F. R. III, "Measurement of acoustic stop bands in two-dimensional periodic scattering arrays," J. Acoustical Soc. Am. **104**(2), 694–699 (1998).
31. A. Khelif, B. Djafari-Rouhani, J. O. Vasseur, and P. A. Deymier, "Transmission and dispersion relations of perfect and defect-containing waveguide structures in phononic band gap materials," Phys. Rev. B **68**(2), 024,302 (2003).
32. A. Dorsel, J. McCullen, P. Meystre, E. Vignes, and H. Walther, "Optical Bistability and Mirror Confinement Induced by Radiation Pressure," Phys. Rev. Lett. **51**(17), 1550–1553 (1983).
33. P. Meystre, E. M. Wright, J. D. McCullen, and E. Vignes, "Theory of radiation-pressure-driven interferometers," J. Opt. Soc. Am. B **2**(11), 1830–1840 (1985).
34. S. G. Johnson, M. Ibanescu, M. A. Skorobogatiy, O. Weisberg, J. D. Joannopoulos, and Y. Fink, "Perturbation theory for Maxwell's equations with shifting material boundaries," Phys. Rev. E **65**(6), 066611 (2002).
35. B.-S. Song, S. Noda, T. Asano, and Y. Akahane, "Ultra-high-Q photonic double-heterostructure nanocavity," Nature Materials **4**, 207–210 (2005).
36. MIT Photonic Bands (MPB) is a free software package for the solution of the electromagnetic eigenmodes of periodic structures. MPB has been developed at MIT, http://ab-initio.mit.edu/wiki/index.php/MPB.
37. COMSOL is a multiphysics software package for performing finite-element-method (FEM) simulations. See COMSOL AB, http://www.comsol.com/. We use the COMSOL multiphysics software package to perform both optical and mechanical numerical simulations of the optomechanical crystal systems.
38. M. Eichenfield, R. Camacho, J. Chan, K. J. Vahala, and O. Painter, "A picogram- and nanometre-scale photonic-

#115150 - $15.00 USD Received 3 Aug 2009; revised 14 Sep 2009; accepted 22 Sep 2009; published 20 Oct 2009

crystal optomechanical cavity," Nature **459**(7246), 550–555 (2009).
39. K. Srinivasan and O. Painter, "Momentum space design of high-Q photonic crystal optical cavities," Opt. Express **10**(15), 670–684 (2002).
40. B. A. Auld, *Acoustic Fields in Waves and Solids* (Robert E. Krieger Publishing Company, 1973).
41. C. Sauvan, P. Lalanne, and J. P. Hugonin, "Slow-wave effect and mode-profile matching in photonic crystal microcavities," Phys. Rev. B **71**, 165118 (2005).
42. P. Velha, J. C. Rodier, P. Lalanne, J. D. Hugonin, D. Peyrade, E. Picard, T. Charvolin, and E. Hadji, "Ultracompact silicon-on-insulator ridge-waveguide mirrors with high reflectance," Appl. Phys. Lett. **89**, 171121 (2006).
43. A. R. Md Zain, N. P. Johnson, M. Sorel, and R. M. De La Rue, "Ultra high quality factor one-dimensional photonic crystal/photonic wire micro-cavities in silicon-on-insulator (SOI)," Opt. Express **16**(16), 084–089 (2008).
44. M. W. McCutcheon and M. Lončar, "Design of a silicon nitride photonic crystal nanocavity with a Quality factor of one million for coupling to a diamond nanocrystal," Opt. Express **16**(23), 136–145 (2008).
45. M. Notomi, E. Kuramochi, and H. Taniyama, "Ultrahigh-Q Nanocavity with 1D Photonic Gap," Opt. Express **16**(15), 905–102 (2008).
46. P. B. Deotare, M. W. McCutcheon, I. W. Frank, M. Khan, and M. Lončar, "Coupled photonic crystal nanobeam cavities," Appl. Phys. Lett. **95**(3), 031,102–3 (2009).
47. P. B. Deotare, M. W. McCutcheon, I. W. Frank, M. Khan, and M. Lončar, "High quality factor photonic crystal nanobeam cavities," Appl. Phys. Lett. **94**(12), 121106 (pages 3) (2009).
48. O. Painter, K. Srinivasan, and P. E. Barclay, "A Wannier-like equation for photon states of locally perturbed photonic crystals," Phys. Rev. B **68**, 035,214 (2003).
49. T. Gorishnyy, J.-H. Jang, C. Koh, and E. L. Thomas, "Direct observation of a hypersonic band gap in two-dimensional single crystalline phononic structures," Appl. Phys. Lett. **91**(12), 121915 (pages 3) (2007).
50. M. S. Kushwaha, P. Halevi, L. Dobrzynski, and B. Djafari-Rouhani, "Acoustic band structure of periodic elastic composites," Phys. Rev. Lett. **71**(13), 2022–2025 (1993).
51. F. R. Montero de Espinosa, E. Jiménez, and M. Torres, "Ultrasonic Band Gap in a Periodic Two-Dimensional Composite," Phys. Rev. Lett. **80**(6), 1208–1211 (1998).
52. A. Cleland, *Foundations of Nanomechanics* (Springer-Verlag, 2003).
53. H. Kolsky, *Stress waves in solids* (Dover Publications, Inc., 1963).
54. B. H. Houston, D. M. Photiadis, M. H. Marcus, J. A. Bucaro, X. Liu, and J. F. Vignola, "Thermoelastic loss in microscale oscillators," Appl. Phys. Lett. **80**(7), 1300–1302 (2002).
55. Y. Yi, "Geometric effects on thermoelastic damping in MEMS resonators," J. Sound Vibration **309**(3-5), 588 – 599 (2008).
56. A. Duwel, J. Gorman, M. Weinstein, J. Borenstein, and P. Ward, "Experimental study of thermoelastic damping in MEMS gyros," Sensors Act. A: Physical **103**(1-2), 70 – 75 (2003).
57. R. Lifshitz and M. L. Roukes, "Thermoelastic damping in micro- and nanomechanical systems," Phys. Rev. B **61**(8) (2000).
58. L. Landau and G. Rumer, "On the absorption of sound in solids," Phys. Zeit. Sowjet. **11**(18) (1937).
59. W. Fon, K. C. Schwab, J. M. Worlock, and M. L. Roukes, "Phonon scattering mechanisms in suspended nanostructures from 4 to 40 K," Phys. Rev. B **66**(4) (2002).
60. T. A. Read, "The Internal Friction of Single Metal Crystals," Phys. Rev. **58**(4) (1940).
61. D. Bindel and S. Govindjee, "Elastic PMLs for resonator anchor loss simulation," Tech report UCB/SEMM-2005/01. Submitted to IJNME **64**(6), 789–818 (2005).
62. M. Maldovan and E. Thomas, "Simultaneous complete elastic and electromagnetic band gaps in periodic structures," Appl. Phys. B **83**(4), 595–600 (2006).
63. S. Mohammadi, A. A. Eftekhar, and A. Adibi, "Large Simultaneous Band Gaps for Photonic and Phononic Crystal Slabs," in *Conference on Lasers and Electro-Optics/Quantum Electronics and Laser Science Conference and Photonic Applications Systems Technologies*, p. CFY1 (Optical Society of America, 2008).

1. Introduction

It has previously been shown that "defects" in a planar periodic dielectric structure can simultaneously confine optical and mechanical resonances to sub-cubic-wavelength volumes[1]. As the co-localized resonances share the same lattice, and thus the same wavelength, the ratio of the optical to mechanical frequency of these modes is proportional to the ratio of their velocities. More recently, it was demonstrated that such co-localized resonances in a silicon structure can strongly couple, via motion-induced phase modulation of the internal optical field, resulting in sensitive optical read-out and actuation of mechanical motion at GHz frequencies[2]. In this paper we aim to further develop the theory and design of these coupled photonic and phononic systems, laying the groundwork for what we term "optomechanical crystals". Here we choose

#115150 - $15.00 USD Received 3 Aug 2009; revised 14 Sep 2009; accepted 22 Sep 2009; published 20 Oct 2009

a cavity-centric viewpoint of the interaction between photons and phonons, using the terminology and metrics from the field of cavity optomechanics [3, 4, 5]. An alternative viewpoint, more appropriate for guided-wave structures, may also be taken in which the interactions are described from a nonlinear optics (Raman-like scattering) perspective [6, 7].

We focus on two cavity devices in particular, a quasi-one-dimensional (quasi-1D) patterned nanobeam and a quasi-two-dimensional (quasi-2D) patterned nanomembrane, both of which have been studied extensively in the past[8, 9] for their photonic properties. The strength of the (linear) optomechanical coupling in such structures is found to be extremely large. Comparisons of optomechanical coupling should be made in comparison to their fundamental limit, which can be arrived at by considering a canonical cavity optomechanical system, the Fabry-Perot with a deformable mirror. Since twice the photon momentum is transfered every round trip, and the round trip length is limited to half an optical wavelength, the limit of cavity optomechanical coupling can be seen to be "diffraction limited" to every photon transferring twice its momentum every optical cycle[10]. The structures presented in this work approach this fundamental limit. Simultaneously, the effective motional mass[11] of the highly confined phonon modes is small, less than few hundred femtograms for a cavity system operating at a wavelength of 1.5 μm and a mechanical frequency of 2 GHz. This combination of parameters makes possible the optical transduction of high-frequency (multi-GHz) mechanical vibrations[12, 7, 13, 6] with near quantum-limited displacement sensitivity[14, 15]. Additionally, dynamical back-action[16] between the photon and phonon fields can be used to dampen[17, 18, 19, 20, 21] and amplify[22, 23, 24] mechanical motion, providing an optical source of coherent phonons[25, 26] which can then be used within other phononic circuit elements[27, 28, 29, 30, 31]. Planar optomechanical crystals then, should enable a new generation of circuits where phonons and photons can be generated, routed, and made to interact, all on a common chip platform.

Unlike the simple motion of a mirror on a spring in more conventional cavity optomechanical systems[32, 33], the complex mechanics of optomechanical crystal structures makes it difficult to intuit the origin or strength of the optomechanical coupling. Nonetheless, understanding the nature of the coupling is crucial to the engineering of optomechanical crystal devices as the degree of coupling between different optical and mechanical mode pairs can vary by orders of magnitude within the same structure, with even subtle changes in the geometry inducing large changes in the optomechanical coupling. In the experimental demonstration of a nanobeam optomechanical crystal[2], it was shown that the perturbation theory of Maxwell's equations with shifting material boundaries [34] provides an accurate method of estimating the optomechanical coupling of these complex motions. Here we describe how this perturbation theory can be used to create an intuitive, graphical picture of the optomechanical coupling of simultaneously localized optical and mechanical modes in periodic systems.

The outline of the paper is as follows. We first analyze the quasi-1D nanobeam optomechanical crystal system. This nanobeam structure provides a simple example through which the salient features of optomechanical crystals can be understood. The mechanical Q of the structure is modeled using absorbing regions that provide a radiation condition for outgoing mechanical vibrations. The various types of mechanical losses are analyzed, and methodologies for minimizing or avoiding these losses are discussed. The dispersive coupling between the optical and mechanical modes is studied next. We use the aforementioned perturbation theory to analyze the optomechanical coupling strength, and which we display as an optomechanical coupling density on the surface of the structure. We use the density of optomechanical coupling picture to illustrate how the structure can be optimized to maximize the optomechanical coupling. Finally, we analyze the optomechanical coupling of a quasi-2D membrane structure, the well-known double-heterostructure photonic crystal cavity [35]. We show how the optical and

#115150 - $15.00 USD Received 3 Aug 2009; revised 14 Sep 2009; accepted 22 Sep 2009; published 20 Oct 2009

mechanical modes and their coupling can be understood in terms of the quasi-one-dimensional nanobeam example.

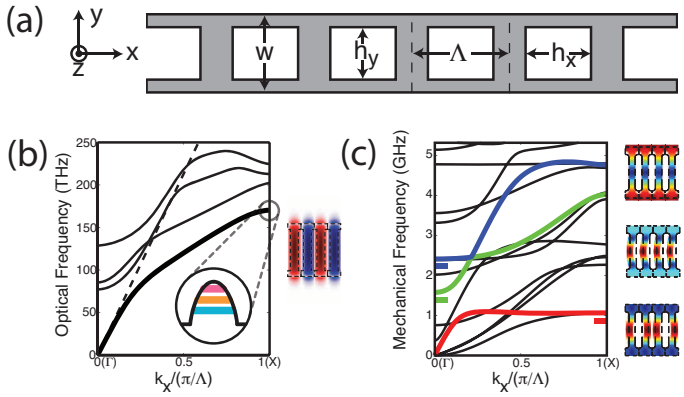

Fig. 1. **(a)** General geometry of the periodic nanobeam structure's projection (infinite structure, no defect). **(b)** Optical band diagram of the nanobeam's projection. The band from which all localized optical modes will be derived is shown in dark black, with E_y of the optical mode at the X point shown to the right of the diagram. The harmonic spatial potential created by the defect, along with the first three optical modes are shown as emanating from the X-point band-edge. **(c)** Mechanical band diagram of the nanobeam's projection. The three bands that can form optomechanically coupled mechanical defect modes are colored. The bottom-most mode is from the X point of the red band; the Γ points of the green and blue bands correspond to the middle and top mechanical modes, respectively. The frequencies of the defect modes that form from the band edges are shown as short, horizontal bars.

2. One-dimensional optomechanical crystal systems: an example

To illustrate the nature of the optomechanical coupling and losses in OMCs, we will use a quasi-1D nanobeam structure which has been demonstrated experimentally[2]. Figure 1(a) shows the general geometry of a periodic, quasi-one-dimensional OMC system made in a silicon beam of nanoscale cross-section. The system consists of an infinitely periodic array of h_x by h_y rectangular holes with center-to-center spacing, Λ, in a beam of width w and thickness, t (not shown). Although the actual structure will employ a defect to localize energy to a small portion of the beam, it is useful to consider the modes of this infinitely-periodic structure. Since the structure has discrete translational invariance, the optical and mechanical modes of the system can be classified according to their wavevector, k_x, and a band index. We shall call the infinitely-periodic structure the *projection* of the system. The band picture provided by the projection allows a simple description of localized optical and mechanical modes as existing between two "mirrors" in which propagating modes at the frequency of the defect have a small or vanishing density of states; the mirrors surround a perturbation region where propagation at the modal frequency is allowed, localizing the propagating mode between the mirrors. The optical and mechanical bands of the OMC's projection are shown in Fig. 1(b) and 1(c), respectively, for the structure $\Lambda = 360$ nm, $w = 1400$ nm, $h_y = 990$ nm, $h_x = 190$ nm, and $t = 220$ nm. The material properties are parameterized by an isotropic Young's modulus, $E = 169$ GPa, Poisson's ratio, $\nu = 0.28$, and index of refraction, $n = 3.49$. The optical bands are computed with the MIT Photonic Bands package[36], while the mechanical bands are computed with COMSOL

#115150 - $15.00 USD Received 3 Aug 2009; revised 14 Sep 2009; accepted 22 Sep 2009; published 20 Oct 2009

Multiphysics[37], a finite element method (FEM) solver. The structure does not possess a complete stop band for either the mechanics or the optics; nevertheless a defect in this structure can simultaneously produce highly-confined, low-loss optical and mechanical modes.

The primary optical band of interest will be the first TE-like (dominantly polarized in the *y*-direction) "valence" band, specifically at the edge of the first Brillioun zone (the edge of the first Brillioun zone is called X and the origin is called Γ). The electric field profile, E_y, is shown next to the band diagram. As described in detail in previous work on "zipper" optomechanical resonators[38, 10] using general momentum-space design rules of photonic crystal cavities[39], the localized modes that come from this band-edge mode are as far as possible from the light line while having a minimal amount of momentum near $k_x = 0$ (and identically zero momentum at $k_x = 0$) when used with a defect that is symmetric about a hole in the center. This reduces the radiation loss out of the structure and is the governing principle behind the optical design of the structure.

Unlike light, mechanical energy cannot radiate into the vacuum. This makes the design rules for creating low-loss mechanical defect modes qualitatively different than those discussed above for optical defect modes. Just as true *photonic* band-gaps are not necessary to achieve high confinement and low optical losses in nanowire structures, true *phononic* bandgaps are also unnecessary to achieve low mechanical losses. A quasi-stop-band, where a defect mode of a particular polarization, frequency, and *k*-vector cannot couple a *significant* amount of energy to the waveguide modes of the mirror portions will be enough to achieve mechanical energy localization.

Many of the most important optomechanical properties of the system are determined by the symmetries of the mechanical modes. Thus it is useful to consider the symmetries of the acoustic eigenmodes of the projection in more detail. The equation of motion for the displacement field, $\mathbf{Q}(\mathbf{r})$, of a non-piezoelectric body is given by[40]

$$\nabla \cdot \left(\mathbf{c} : \nabla_s \mathbf{Q}(\mathbf{r})\right) = \rho \frac{\partial^2 \mathbf{Q}(\mathbf{r})}{\partial t^2} \,, \tag{1}$$

where $\nabla_s \equiv \left(\nabla + \nabla^T\right)/2$ is the symmetric gradient operator, ρ is the mass density, the colon denotes the double scalar (a.k.a. double dot) product of a fourth rank and a second rank tensor, and $\mathbf{c}$ is the (fourth rank) elasticity tensor. As we are treating the material as isotropic, the elasticity tensor reduces in Voigt notation to[40]

$$\mathbf{c}^{-1} = \frac{1}{E}\begin{bmatrix} 1 & -\nu & -\nu & 0 & 0 & 0 \\ -\nu & 1 & -\nu & 0 & 0 & 0 \\ -\nu & -\nu & 1 & 0 & 0 & 0 \\ 0 & 0 & 0 & 2(1+\nu) & 0 & 0 \\ 0 & 0 & 0 & 0 & 2(1+\nu) & 0 \\ 0 & 0 & 0 & 0 & 0 & 2(1+\nu) \end{bmatrix}, \tag{2}$$

where E is Young's modulus and ν is Poisson's ratio.

The projection of the nanobeam optomechanical crystal (the infinite extension of the structure without the defect) has discrete periodicity, satisfying $\mathbf{Q}(\mathbf{r}) = \mathbf{Q}(\mathbf{r} + \Lambda\hat{\mathbf{x}})$, where Λ is the periodicity of the lattice. Thus, by Bloch's theorem, the solutions can be classified according to a wavevector, k_x, in the first Brillouin zone, $k_x \in [-\pi/\Lambda, \pi/\Lambda]$ (time-reversal symmetry guarantees that positive and negative wavevectors yield identical solutions, and the solutions can further be restricted to the first half of the first Brillouin zone, $k_x \in [0, \pi/\Lambda]$) . As the Bloch solution is effectively restricted to a finite region of space (the unit cell), the solutions for a given k_x have a discrete spectrum of eigenfrequencies, which can be labeled by a band index, n. Furthermore, the structure is mirror symmetric about the $y = 0$ and $z = 0$ planes (see Fig. 2),

#115150 - $15.00 USD Received 3 Aug 2009; revised 14 Sep 2009; accepted 22 Sep 2009; published 20 Oct 2009

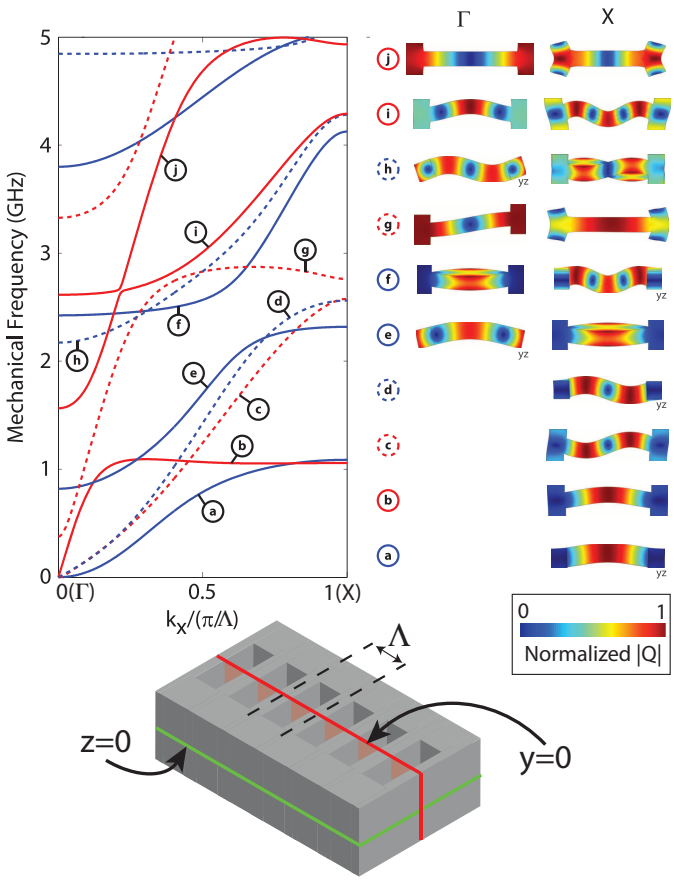

Fig. 2. Mechanical band diagram and corresponding normalized displacement profiles of the unit cell at the Γ ($k_x = 0$) and X ($k_x = \pi/\Lambda$) points. In the band diagram, the mirror symmetry σ_z, (across the plane defined by $z = 0$) is indicated by color: red corresponds to even vector parity ($p_z = 1$) and blue to odd vector parity ($p_z = -1$). Mirror symmetry σ_y (across the plane defined by $y = 0$) plane is indicated by the line shape: solid corresponds to even vector parity ($p_y = 1$) and dashed to odd vector parity ($p_y = -1$). The mechanical mode profiles are all viewed from a direction normal to the $z = 0$ plane unless labeled "yz", in which case the viewing angle is normal to the $x = 0$ plane. The pinch, accordion, and breathing mode bands are b, i, and j, respectively. As torsional modes can be difficult to interpret without isometric views, it is noted for the reader that the mechanical modes for band e at X, band f at Γ, and band h at X are all torsional mechanical modes.

and it can be shown that the mirror operators,

$$\sigma_y = \begin{bmatrix} 1 & 0 & 0 \\ 0 & -1 & 0 \\ 0 & 0 & 1 \end{bmatrix} \quad \sigma_z = \begin{bmatrix} 1 & 0 & 0 \\ 0 & 1 & 0 \\ 0 & 0 & -1 \end{bmatrix}, \tag{3}$$

commute with the differential operator $\Xi \equiv \nabla \cdot \mathbf{c} : \nabla_s$. The solutions to the wave equation can thus be further classified with respect to their vector parity about these planes, each solution having an eigenvalue of the mirror operator such that $\sigma_j \mathbf{Q}(\sigma_j^{-1}\mathbf{r}) = p_j \mathbf{Q}(\mathbf{r})$ (note that

#115150 - $15.00 USD Received 3 Aug 2009; revised 14 Sep 2009; accepted 22 Sep 2009; published 20 Oct 2009

$\sigma_j^{-1} = \sigma_j$), where j can be y or z, and $p_j = \pm 1$. We accordingly classify the solutions to the wave equation by the wavevector $k_x \in [0, \pi/\Lambda]$, p_y, and p_z. Figure 2 shows the mechanical band diagram of the nanobeam optomechanical crystal's projection, with the first ten band indices labeled a to j, p_z indicated by color, and p_y indicated by line shape. The mechanical displacement profiles of the unit cell are shown for each band at Γ and X.

Two important points about the symmetries of the mechanical bands must be made. First, any "defect" that preserves the σ_y and σ_z symmetries will create localized modes that also have these symmetries. Since the localized modes of a defect can be viewed as being drawn from the band edges of the projection, a defect mode drawn from a band of one symmetry cannot couple to a mode of the projection outside the defect that has a different symmetry. This creates *effective* bandgaps even though the structure does not possess any *complete* bandgaps. Second, it will turn out that, for the nanobeam structure, the total optical dispersion created by any mechanical mode is zero unless the mode has $p_y = p_z = +1$. So although the structure has many acoustic bands that can create localized modes, only those bands with red, solid lines in Fig. 2 can produce localized mechanical modes with optomechanical coupling.

We now consider the localization of the mechanical and optical modes by the defect. We start by considering the optical modes. Because of the finite index contrast of the system, the optical Q of localized modes is limited by radiation from optical momentum components that are close to $k_x = 0$, since the system can only guide momentum components that are above the critical angle for total internal reflection. This governs the design of the defect and choice of localized optical modes of the structure. Clearly only bandedges lying outside the light cone can be guided by the structure, which limits the useful bandedges to those at the X point. As discussed above, the fundamental optical band at the X point is the farthest from the light line and produces the most localized modes of the defect. Because this optical band has negative curvature at the X point, the frequency of the mode at the band edge must be increased to confine an optical mode coming from this band. This can be accomplished by decreasing Λ (making the holes closer together without changing the size of the hole). As has been shown [41, 42, 43, 44, 45, 10, 38, 46, 47] both theoretically and experimentally, these nanobeam systems are capable of achieving very high radiation-limited Q-factors.

Unlike the optical bands, all mechanical modes are "guided" by the structure, regardless of their k-vector, which allows localized mechanical modes to be created from bandedges at either of the high symmetry points, Γ or X. In fact, it will be shown that it is advantageous to draw mechanical modes from the Γ point, as this generally produces larger optomechanical coupling than drawing from X. Clearly the mechanical mode should be localized by the same defect as the optical mode; if this is not the case, then the target mechanical band-edge should be essentially unaffected by the defect that creates the optical mode, and a separate defect must be found that can localize the mechanics without significantly affecting the optical mode. As this is clearly more complicated, we will employ a defect that strongly confines both optical and mechanical modes simultaneously. Finally, the localized defect mode that is formed from the band edge must be sufficiently optomechanically coupled to the localized optical mode(s) of interest.

The exact defect that will be employed to localize optical and mechanical energy to the center of the structure consists of a decrease in the lattice constant for the otherwise periodic array of N_{total} holes in the beam, as illustrated in Fig. 3(c). As discussed above, for the modes that are localized by the defect, this effectively divides the structure into a defect portion where propagation is allowed, surrounded by mirrors, where the localized modes are evanescent. The particular defect used here consists of some odd number of holes, N_{D}, with the spacing between the holes varying quadratically from the background lattice constant, Λ, to some value Λ_{D}, with the spacing varying symmetrically about the center hole (the hole dimensions are held

#115150 - $15.00 USD Received 3 Aug 2009; revised 14 Sep 2009; accepted 22 Sep 2009; published 20 Oct 2009

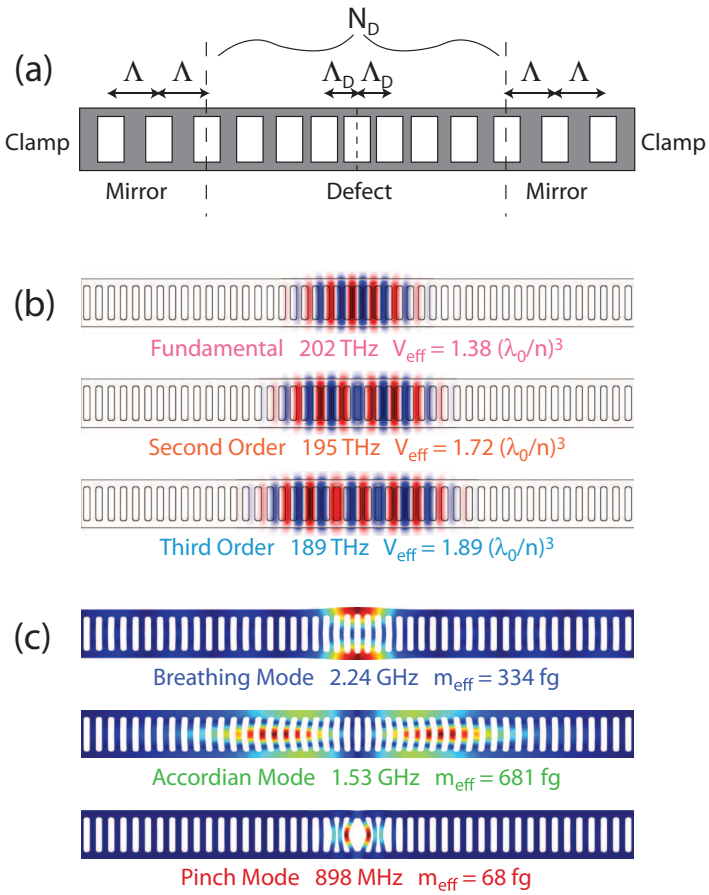

Fig. 3. **(a)** Schematic illustration of actual nanobeam optomechanical crystal with defect and clamps at substrate. **(b)** Localized optical modes of the nanobeam OMC. The colors of the names correspond to the illustration of the inverted potential in Fig. 1(b). Localized, optomechanically-coupled mechanical modes of the nanobeam OMC. The colors of the names correspond to the colored bands and horizontal bars showing the modal frequencies in Fig. 1(c).

fixed throughout the structure). The complete geometry, which we will refer to as "the nominal structure" is: $N_{\text{total}} = 75$, $\Lambda = 360$ nm, $w = 1400$ nm, $h_y = 990$ nm, $h_x = 190$ nm, $t = 220$ nm, $N_{\text{D}} = 15$, and $\Lambda_{\text{D}} = 0.85\Lambda$.

With regard to the symmetries of the mechanical bands discussed above, the defect in the structure breaks the discrete periodicity in the x direction, and the solutions to the wave equation (Eq. (1)) for the structure can no longer be classified by wavevectors and band indices. The structure still retains its σ_y and σ_z mirror planes. In addition, the structure now has a third mirror plane (the plane $x = 0$), which divides the structure in half in the x direction. As with the solutions of the projection, the wave equation commutes with the mirror operator σ_x, where

$$\sigma_x = \begin{bmatrix} -1 & 0 & 0 \\ 0 & 1 & 0 \\ 0 & 0 & 1 \end{bmatrix}. \tag{4}$$

#115150 - $15.00 USD Received 3 Aug 2009; revised 14 Sep 2009; accepted 22 Sep 2009; published 20 Oct 2009

Each solution of the wave equation is thus an eigenvector of σ_j, with corresponding vector parity $p_j = \pm 1$, $j \in [x,y,z]$.

The solutions to the wave equation in the defect can be viewed as being drawn from the band edges of the projection. Localized modes are formed whenever the modes of the defect exist at a frequency for which the density of states in the projection is small or zero. Thus, many localized mechanical modes are formed at the various band edges.

For localized optical and mechanical modes, the quasi-harmonic spatial defect creates a quasi-harmonic potential for optical and mechanical mode envelopes [48] composed of modes near the band edge. This creates a ladder of states for each band edge with approximately Hermite-Gauss spatial dependencies along the cavity axis (x), in direct analogy to the harmonic potential of 1D quantum mechanics. As discussed above, the localized optical modes of interest come entirely from a single band-edge (the darkened band in Fig. 1(b)); the first three cavity modes of the defect from that band are shown in Fig. 3(b). Manifolds of localized acoustic modes also form for many bandedges, such as the breathing modes drawn from band "j" in Fig. 2. These manifolds are composed of modes having identical parities with respect to σ_y and σ_z, and the parity with respect to σ_x alternates as one climbs the ladder of states in the manifold. It was previously mentioned that only bands with $p_y = p_z = +1$ can form defect modes with optomechanical coupling. In fact, the defect modes must also have $p_x = +1$ to have optomechanical coupling. The solid red bands in Fig. 2 form localized modes at the bandedges, and the mode manifolds alternate between modes with and without optomechanical coupling. As examples of localized mechanical modes with optomechanical coupling, we will examine three different optomechanically-coupled mechanical cavity modes, each derived from a different mode at the band edge, even though each of these band-edge modes produces a manifold of defect modes which may or may not have optomechanical coupling. These modes are shown in Fig. 3(c) and are given descriptive names that highlight the nature of the mechanical motion: "pinch", "accordion", and "breathing". The fact that the optomechanical coupling vanishes for all modes except those with $p_x = p_y = p_z = +1$ will be made more explicit in the description of optomechanical coupling below.

3. Modal cross-coupling and mechanical losses

Periodic structures can be fabricated to have phononic band gaps[49, 50, 30, 51], where mechanical energy loss by linear elastic coupling to the environment can be made arbitrarily small. Eventually, more fundamental losses[52, 53] such as thermoelastic loss[54, 55, 56, 57], non-equilibrium energy redistribution[58, 53], phonon-phonon scattering[59], and the movement of dislocations and impurities[60, 53] should be accessible in these systems. First, however, the linear interaction of the optomechanical crystal and its surrounding substrate, which acts as a bath, must be understood and minimized. With this in mind, we use a finite element method model with weakly absorbing "bath" regions to model the losses in the system due to coupling of the mechanical energy into modes that are not confined. This method captures inter-modal coupling between the localized modes and all other mechanical modes of the system, some of which act as parasitic loss channels into the surrounding "bath".

The lack of a mechanical bandgap means that the superposition of k-vectors necessary to create a localized mode in the defect coincide with k-vectors of equi-frequency propagating modes of the phononic crystal mirrors. The localized modes and propagating modes of equal frequency will hybrizide and couple whenever the symmetries of the modes (see discussion above) do not forbid it. In addition to the propagating modes, there are "body modes" that exist purely because of the boundary conditions (and thus not represented in the band structure), such as vibrations, density waves, and torsions of the finite, clamped structure. If the simulated exterior boundary conditions allow energy in the propagating and body modes to be lost, the

#115150 - $15.00 USD Received 3 Aug 2009; revised 14 Sep 2009; accepted 22 Sep 2009; published 20 Oct 2009

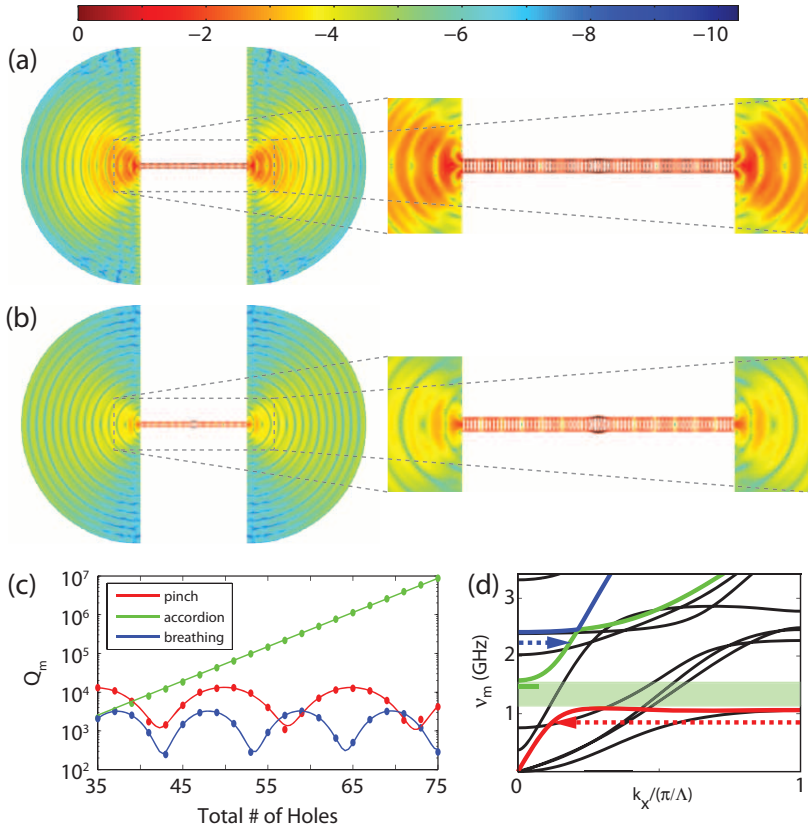

Fig. 4. **(a)** In-phase and **(b)** in-quadrature mechanical displacement field ($\log_{10}(|\mathbf{q}|^2/\max(|\mathbf{q}|^2)$) of the fundamental breathing mode of nanobeam OMC structure with weakly absorbing "pad", showing the propagating nature of the radiated mechanical waves in the pad region. **(c)** Dependence of Q_m on the total length of the structure; the number of mirror holes on each side is $(N_T - 15)/2$. This shows the oscillatory Q_m of the pinch and breathing modes, which are coupled to waveguide modes, and the exponentially-increasing Q_m of the accordion mode. **(d)** Mechanical band structure of the nanobeam OMC, with arrow tails indicating the frequency and high-symmetry point of the breathing (blue) and pinch (red) modes, and arrow heads indicating the equi-frequency waveguide mode that acts as the dominant source of parasitic coupling. The effective bandgap of the accordion mode is shown in transparent green, with its frequency indicated as a horizontal green bar at the Γ point.

propagating and body modes that couple to the localized mode will act as parasitic loss channels for the localized mode.

In a fabricated structure, the cantilever is attached to a substrate at both ends, rather than a hard boundary at the end of the cantilever. These more realistic boundaries must be included to model propagating and body mode losses. The propagating modes travel down the nanobeam and partially reflect at the contacts due to an effective impedance mismatch caused by the geometric change between the nanobeam and the bulk. The rest of the power radiates into the bulk, causing a loss of mechanical energy. Thus the localized mode is coupled to a propagating mode with identical frequency that can radiate part or all of its energy into the surrounding "bath".

#115150 - $15.00 USD Received 3 Aug 2009; revised 14 Sep 2009; accepted 22 Sep 2009; published 20 Oct 2009

This propagating mode also forms a coupled cavity resonance with the localized mode because of the reflections at the clamp points. The body modes have a softer boundary condition than $\mathbf{q} = 0$ at the boundaries, extending the body mode amplitude into the substrate. The part of the body mode that extends into the substrate can excite radiative modes of the substrate. The body mode then acts as a loss channel for any localized mode to which it is coupled. The localized, propagating, and body modes form a set of coupled resonators. Since the body and propagating modes are very sensitive to the total length of the structure, the self-consistent solution, which determines the loss of the localized mode, is very sensitive to the exact boundary conditions. Thus, to accurately simulate the true spatial profiles and losses of localized mechanical modes, one needs a simulation that reflects the true boundary conditions.

To model the loss due to coupling to radiative modes of the substrate, we include a large, semi-circular "pad" on each side of the nanobeam, with the same material constants as the nanobeam. To make the pad act like a "bath", we introduce a phenomenological imaginary part of the speed of sound in the pad region; i.e., $\mathrm{v}_{\mathrm{pad}} \rightarrow \mathrm{v}_{\mathrm{Silicon}}(1 + i\eta)$, where $\mathrm{v} = \sqrt{E/\rho}$. This creates an imaginary part of the frequency, and the mechanical Q can be found by the relation, $Q_{\mathrm{m}} = \mathrm{Re}\{\nu_{\mathrm{m}}\}/(2\mathrm{Im}\{\nu_{\mathrm{m}}\})$. By adding loss to the pad material, propagating modes will reflect part of their power at the contacts (the interface between the cantilever and the substrate) because of the change in the impedance from the absorption, not just the geometric change in impedance. From this point of view, η should be made as small as possible, since this contribution to the reflection coefficient is an artifact of the simulation and is not present in the real system. However, η must also be large enough that the self-consistent solution includes a propagating, radiated wave, which only happens if the wave is appreciably attenuated by the time it reflects from the edge of the simulation (where $\mathbf{q} = 0$) and returns to the contact. Thus, the pad is made as large as possible, given computational constraints, and the absorption is increased until Q_{m} changes appreciably, which gives the threshold value for η at which the reflectivity of the contacts has an appreciable contribution from the absorption. The simulation is then performed with a value of η that produces a propagating wave in the pad without causing an artificial reflectivity at the contact. Propagation in the pad is easily verified if the position of the nodes/antinodes swap between the in-phase and in-quadrature parts of the mechanical cycle (the nodes/antinodes of a standing wave are stationary). Figure 4(a) and 4(b) show the in-phase and in-quadrature (respectively) parts of the mechanical cycle of the breathing mode, clearly showing a propagating radiative mode in the weakly absorbing pad, with $\log_{10}(|\mathbf{q}|^2/\max(|\mathbf{q}|^2)$ plotted to elucidate the attenuation of mechanical radiation in the pad.

Limiting the artificial reflection at the interface of the non-absorbing and absorbing portions sets the maximum absorptivity, which in turn sets the minimum size of the pad (to guarantee that the radiation is completely attenuated before returning to the contact). This size/absorptivity trade-off can be improved by making η vary as a function of position in the pad, starting out at zero and increasing radially outward (quadratically, say). This is analogous to a mechanical perfectly matched layer (PML)[61], which has the benefit of increasing the round-trip absorption while maintaining a minimum reflectance at the clamp *due to* absorption. This provides the same reflection-free absorption of mechanical radiation in a more compact simulation space, making better use of computational resources.

Changing the length of the structure changes the resonance condition for both the propagating and body modes. This changes the amount of coupling to the localized mode in the self-consistent solution of the system. Thus the parasitic losses into a waveguide mode should be periodic. Figure 4(c) shows Q_{m} for the pinch, accordion, and breathing mode as the total number of holes (i.e., the length of the optomechanical crystal) is varied. For the breathing and pinch modes, the mechanical losses oscillate as a function of the total length of the nanobeam. For this particular geometry, the losses are dominated by propagating modes, and the oscilla-

#115150 - $15.00 USD Received 3 Aug 2009; revised 14 Sep 2009; accepted 22 Sep 2009; published 20 Oct 2009

tion period of the Q can be matched to a k-vector of a waveguide mode in the band structure in Fig. 4(d) (shown as a dotted line extending from the defect frequency). Thus the length of the structure can be tuned to minimize mechanical losses in cases where a complete mechanical bandgap is not present. Interestingly, the Q of the accordion mode increases exponentially with the number of holes, indicating that the mode is evanescent in the mirror portions. Examining the four bands that cross through at the frequency of the accordion mode (see Fig. 2), we find that all four bands have a mirror symmetry about either the $x-z$ or $x-y$ planes that forbids any hybridization between or coupling to the accordion mode. This creates an effective bandgap (shown in translucent green). Practically speaking, this is a much weaker stop-band than a true bandgap, because any defect in the structure that breaks the symmetry of the accordion mode about the mirror planes will cause a coupling to the waveguide modes in the gap. However, it is exactly this kind of symmetry-dependent effective bandgap that is responsible for the high *optical* Q[38, 2, 46, 47] of the experimentally-fabricated structures. This gives some confidence that it is possible to fabricate structures that are defect-free to the degree necessary to achieve high Q_{m}.

4. Optomechanical coupling: definition and integral representation

Cavity optomechanics involves the mutual coupling of two modes of a deformable structure: one optical and one mechanical. The optical mode is characterized by a resonant frequency $\omega_{\mathrm{o}} = 2\pi\nu_{\mathrm{o}}$ and electric field $\mathbf{E}(\mathbf{r})$. The mechanical mode is characterized by a resonant frequency $\Omega_{\mathrm{m}} = 2\pi\nu_{\mathrm{m}}$ and displacement field $\mathbf{Q}(\mathbf{r})$, where $\mathbf{Q}(\mathbf{r})$ is the vector displacement describing perpendicular displacements of the boundaries of volume elements. The cavity optomechanical interactions of the distributed structure and its spatially-dependent vector fields, $\mathbf{E}(\mathbf{r})$ and $\mathbf{Q}(\mathbf{r})$, can be reduced to a description of two *scalar* mode amplitudes and their associated mode volumes, with the coupling of the amplitudes parameterized by a single coupling coefficient, g_{OM}.

The mode amplitude, c, and complex vector field profile, $\mathbf{e}(\mathbf{r})$, are defined such that the complex electric field is $\mathbf{E}(\mathbf{r}) = c\mathbf{e}(\mathbf{r})$ (the physical field is given by the real part of $\mathbf{E}(\mathbf{r})e^{i\omega t}$). For pedagogical reasons, the amplitude c is normalized such that the time averaged electromagnetic energy is equal to $|c|^2$; i.e. $U = |c|^2 = \frac{1}{2}\int \mathrm{d}V\varepsilon\,|\mathbf{E}|^2$. This forces $\mathbf{e}$ to be normalized such that $1 = \frac{1}{2}\int \mathrm{d}V\varepsilon\,|\mathbf{e}|^2$. In cavity quantum electrodynamics, one typically defines an effective optical mode volume, $V_{\mathrm{o}} = \int \mathrm{d}V \left(\frac{\sqrt{\varepsilon}|\mathbf{E}|}{\max\left(|\sqrt{\varepsilon}\mathbf{E}|\right)}\right)^2$, in order to gauge the strength of light-matter interactions.

The mechanical vibration's amplitude, α, and mode profile (displacement), $\mathbf{q}(\mathbf{r})$, are defined such that $\mathbf{Q}(\mathbf{r}) = \alpha\mathbf{q}(\mathbf{r})$. Here, α is defined as the largest displacement that occurs anywhere for the mechanical field, $\mathbf{Q}(\mathbf{r})$, so that $\max(|\mathbf{q}(\mathbf{r})|) = 1$. The mode amplitude, α, must also represent the amplitude of the generalized position, $\beta(t) = \alpha\cos(\Omega t)$, and generalized momentum, $m_{\mathrm{eff}}\dot{\beta}(t)$, of a simple harmonic oscillator with an energy, $E_{\mathrm{mechanical}} = \frac{m_{\mathrm{eff}}}{2}(\Omega^2\beta^2 + \dot{\beta}^2)$. Our particular choice of α determines the mechanical mode's effective volume, V_{m}, and effective mass, $m_{\mathrm{eff}} \equiv \rho V_{\mathrm{m}}$, since this choice of α requires the complimentary definition $m_{\mathrm{eff}} = \rho\int \mathrm{d}V \left(\frac{|\mathbf{Q}|}{\max(|\mathbf{Q}|)}\right)^2$. To see this note that, at the classical turn-around point, integrating the potential energy of each volume element must give the total potential energy. Thus $E_{\mathrm{mechanical}} = \frac{1}{2}\Omega^2\int \rho|\mathbf{Q}(\mathbf{r})|^2\mathrm{d}V = \frac{1}{2}m_{\mathrm{eff}}\Omega^2\alpha^2$, or, in other words, $m_{\mathrm{eff}}\alpha^2 = \int \rho|\mathbf{Q}(\mathbf{r})|^2\mathrm{d}V$. One can arbitrarily choose the definition of the amplitude or the mass, but choosing one determines the other. In addition, α is the amplitude of zero-point motion of the canonical position operator in a quantized treatment. For a system like a localized mode of a phononic crystal defect cavity, where only a very small, localized portion of the total mass undergoes appreciable motion, the

#115150 - $15.00 USD Received 3 Aug 2009; revised 14 Sep 2009; accepted 22 Sep 2009; published 20 Oct 2009

most sensible choice of the mass is the amplitude-squared weighted density integral, which, as stated above, is the choice of mass associated with $\alpha = \max(|\mathbf{Q}(\mathbf{r})|)$.

The optomechanical coupling affects the optical mode by tuning the optical resonant frequency as a function of displacement, $\omega_o(\alpha)$; whereas the coupling affects the mechanical mode by applying a force, which is expressed as a gradient of the cavity energy, $\mathrm{d}|c|^2/\mathrm{d}\alpha$. The optical resonant frequency is usually expanded in orders of the (small) displacement, α around some equilibrium displacement, α_0.

$$\omega_o(\alpha) = \omega_o\Big|_{\alpha=\alpha_0} + (\alpha-\alpha_0)\frac{\mathrm{d}\omega_o}{\mathrm{d}\alpha}\Big|_{\alpha=\alpha_0} + \frac{1}{2}(\alpha-\alpha_0)^2\frac{\mathrm{d}^2\omega_o}{\mathrm{d}\alpha^2}\Big|_{\alpha=\alpha_0} + \ldots \tag{5}$$

In the case that the terms higher than first order can be neglected, this equation simplifies to

$$\omega_o(\alpha) = \omega_o\Big|_{\alpha=\alpha_0} + (\alpha-\alpha_0)\frac{\mathrm{d}\omega_o}{\mathrm{d}\alpha}\Big|_{\alpha=\alpha_0} \equiv \omega_o + (\alpha-\alpha_0)g_{\mathrm{OM}} \equiv \omega_o + (\alpha-\alpha_0)\frac{\omega_o}{L_{\mathrm{OM}}}\,, \tag{6}$$

where $\omega_o \equiv \omega_o\Big|_{\alpha=\alpha_0}$ is the equilibrium resonance frequency of the optical mode, $g_{\mathrm{OM}} \equiv \frac{\mathrm{d}\omega_o}{\mathrm{d}\alpha}\Big|_{\alpha=\alpha_0}$ is the derivative of the resonance frequency of the optical mode evaluated at equilibrium, and L_{OM} is the *effective optomechanical length* of the system. The effective length, L_{OM}, is a universal parameter that relates displacement to a change in optical frequency (i.e. $\alpha/L_{\mathrm{OM}} = \delta\omega_o/\omega_o$). From the definition, $L_{\mathrm{OM}}^{-1} \equiv \frac{1}{\omega_o}\frac{\mathrm{d}\omega_o}{\mathrm{d}\alpha}\Big|_{\alpha=\alpha_0} = g_{\mathrm{OM}}/\omega_0$, one can see that reducing L_{OM} maximizes the optomechanical coupling. Moreover, this optomechanical coupling length is "diffraction limited" to $\lambda_o/(2n_{\mathrm{eff}})$, where λ_o is the free space optical wavelength and n_{eff} is the effective index of the optical mode. It is simple to show that L_{OM} is equal to the spacing between the mirrors of a Fabry-Perot cavity when one mirror is allowed to move along the cavity axis or the radius of a microtoroid/microdisk for a radial breathing motion, which clearly has a lower limit of half the optical wavelength. For a "Zipper" cavity or double-microdisk, L_{OM} is an exponentially decreasing function of the spacing between the coupled elements, with L_{OM} approaching half the effective optical wavelength of light in the material as the *spacing* approaches zero.

The perturbation theory of Maxwell's equations with shifting material boundaries[34] allows one to calculate the derivative of the resonant frequency of a structure's optical modes with respect to some parameterization of a surface deformation, $h(\alpha;\mathbf{r})$, *perpendicular* to the surface of the structure. This results in the derivative of the dispersion with respect to alpha being equal to

$$\frac{\mathrm{d}\omega_o}{\mathrm{d}\alpha} = \frac{\omega_o}{2}\frac{\int \mathrm{d}A\frac{\mathrm{d}h}{\mathrm{d}\alpha}\left[\Delta\varepsilon\left|\mathbf{E}_{\|}\right|^2 - \Delta(\varepsilon^{-1})\left|\mathbf{D}_{\perp}\right|^2\right]}{\int \mathrm{d}V\varepsilon|\mathbf{E}|^2}\,. \tag{7}$$

Thus, if the result of a mechanical simulation is the displacement field, $\mathbf{Q}(\mathbf{r}) = \alpha\mathbf{q}(\mathbf{r}) \equiv \alpha\mathbf{Q}(\mathbf{r})/\max(|\mathbf{Q}|)$, then using the definition of the effective optomechanical coupling length, L_{OM}, and accounting for field normalizations,

$$\frac{1}{L_{\mathrm{OM}}} = \frac{1}{4}\int \mathrm{d}A\,(\mathbf{q}\cdot\hat{\mathbf{n}})\left[\Delta\varepsilon\left|\mathbf{e}_{\|}\right|^2 - \Delta(\varepsilon^{-1})\left|\mathbf{d}_{\perp}\right|^2\right] \tag{8}$$

where $\mathbf{d} = \varepsilon\mathbf{e}$, $\hat{\mathbf{n}}$ is the unit normal vector on the surface of the unperturbed cavity, $\Delta\varepsilon = \varepsilon_1 - \varepsilon_2$, $\Delta(\varepsilon^{-1}) = \varepsilon_1^{-1} - \varepsilon_2^{-1}$, ε_1 is the dielectric constant of the structure, and ε_2 is the dielectric constant of the surrounding medium.

#115150 - $15.00 USD Received 3 Aug 2009; revised 14 Sep 2009; accepted 22 Sep 2009; published 20 Oct 2009

To calculate L_{OM} by deforming the structure, one must simulate the fields with a deformation amplitude, α, that is large enough to be detectable numerically but small enough that higher order dispersion does not affect the frequency shift. To verify that higher order dispersion is not included, one must simulate the optical fields for a range of displacement amplitudes and extract the linear dispersion. Because perturbation theory can calculate the linear term exactly from a single calculation using the *undeformed* structure, this method has clear advantages over numerical methods using finite deformations.

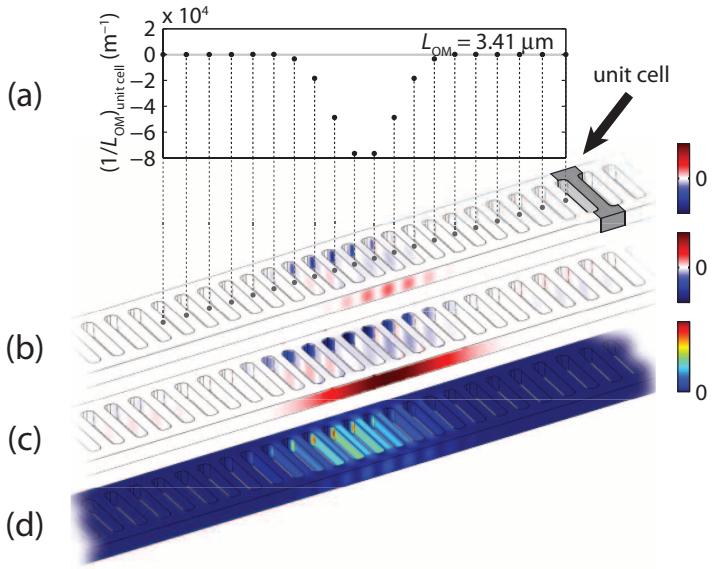

Fig. 5. For the fundamental breathing mode and the fundamental optical mode in the nominal structure, **(a)** FEM simulation of individual unit cell contributions to the total optomechanical coupling (each point computed by integrating ζ_{OM} (Equation 8) over the respective unit cell), **(b)** surface plot of the optomechanical coupling density, ζ_{OM}. **(c)** surface plot of the normal displacement profile, Θ_m (Equation 10), **(d)** surface plot of the electromagnetic energy functional, Θ_o (Equation 11). In (d), there is significant optomechanical coupling density in the corner of the holes, where the crossbar meets the rail. Without the fillets, the field amplitude is concentrated in the corner and difficult to see. For this reason, the corners have been filleted to allow the optomechanical coupling density in the corners to be visualized. The fillets do not significantly affecting the optomechanical coupling (confirmed by simulation).

5. Optomechanical coupling: visual representation and optimization

In addition to being computationally simpler than deformation methods, the perturbative method of calculating the optomechanical coupling allows one to represent the optomechanical coupling as a density on the surface, with different parts of the structure contributing different amounts of optomechanical coupling. This yields much more information than just the value of L_{OM}, itself. The optomechanical coupling density is given by

$$\zeta_{OM}(\mathbf{r}) \equiv \frac{1}{4}(\mathbf{q}\cdot\hat{\mathbf{n}})\left[\Delta\varepsilon\left|\mathbf{e}_{\parallel}\right|^2 - \Delta(\varepsilon^{-1})\left|\mathbf{d}_{\perp}\right|^2\right]. \tag{9}$$

The optomechanical coupling density can further be broken down into a mechanical part (the

#115150 - $15.00 USD Received 3 Aug 2009; revised 14 Sep 2009; accepted 22 Sep 2009; published 20 Oct 2009

normal displacement profile)

$$\Theta_m(\mathbf{r}) \equiv \mathbf{q} \cdot \hat{\mathbf{n}} \tag{10}$$

and an optical part (the electromagnetic energy functional)

$$\Theta_o(\mathbf{r}) \equiv \Delta\varepsilon \left|\mathbf{e}_{\|}\right|^2 - \Delta(\varepsilon^{-1}) \left|\mathbf{d}_{\perp}\right|^2 , \tag{11}$$

which can be separately visualized on the surface. This provides a quantitative method of assessing the separate optical and mechanical contributions and allows an intuitive approach to individually engineering the optical and mechanical properties of the structure to enhance the optomechanical coupling of specific modes.

Figure 5(a) shows the contribution to the optomechanical coupling, L_{OM}^{-1}, of the breathing mode and fundamental optical mode from each "unit cell" of the structure. Summing the contributions from each unit cell yields L_{OM}^{-1}. Figs. 5(b)-(d) show ζ_{OM}, Θ_m, and Θ_o, plotted on the surface of the nanobeam OMC for the fundamental breathing mode and the fundamental optical mode. In Fig. 5(b), it can be seen that there are two dominant and opposite contributions to the optomechanical coupling: one from the outside face of the rails and one from the inside face of the rails (in the corners of holes). Minimizing the cancellation between these two contributions is critical to achieving a small L_{OM} for the breathing mode (i.e. strong optomechanical coupling). The geometry of the "nominal" structure optimizes the coupling between the fundamental optical mode and the breathing mode, as shown below.

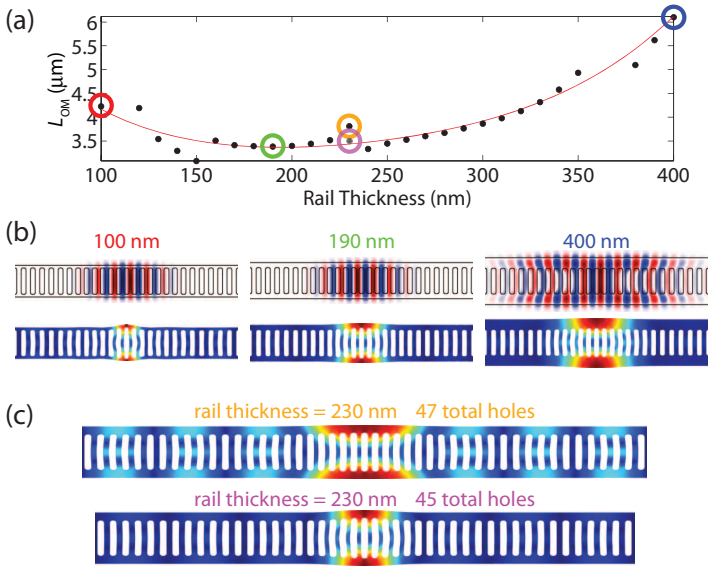

Fig. 6. For the fundamental breathing mode and the fundamental optical mode, **(a)** the dependence of the optomechanical coupling on the rail thickness (with oscillations in the data arising from accidental degeneracies with the cantilever modes), **(b)** the optical and mechanical mode profiles for rail thicknesses of 100 nm, 190 nm and 400 nm circled in red, green and blue respectively in (a), **(c)** comparison of the mechanical mode profiles when coupled (orange) and not coupled (purple) to cantilever modes, with the corresponding effect on in L_{OM} highlighted in (a).

Since the breathing mode is drawn from a band edge at the Γ point, adjacent unit cells are mechanically in-phase with each other and add constructively to the optomechanical coupling.

#115150 - $15.00 USD Received 3 Aug 2009; revised 14 Sep 2009; accepted 22 Sep 2009; published 20 Oct 2009

This is in contrast to defect modes drawn from band edges at the X point, such as the pinch mode, where adjacent unit cells are mechanically out-of-phase, resulting in neighboring unit-cell contributions that tend to cancel. This cancellation reduces the optomechanical coupling unless it is specifically mitigated with extremely tight modal envelopes (see description of pinch mode optomechanical coupling below).

The degree to which the different faces of the rails cancel each other's contribution to L_{OM}^{-1} is set by the attenuation of the optical field between the two edges, as the mechanical displacement of the two rails is fairly uniform. Thus, one would expect that varying the rail thickness, which changes the relative amplitude of the optical field on the two rail faces, would have a significant impact on the coupling. Figure 6(a) shows L_{OM} as a function of rail thickness, with L_{OM} of the nominal structure (190 nm rail thickness) circled in green. For rail thicknesses smaller than 190 nm (such as the 100 nm rail width, circled in red in Fig. 6(a) and shown in Fig. 6(b)), the amplitude of the optical field on the inside and outside edge of the field is becoming more and more similar. This results in a larger cancellation between the contributions to L_{OM}^{-1} on the inside and outside of the rails, decreasing the optomechanical coupling. This reasoning might lead one to believe that increasing the rail thickness should monotonically decrease L_{OM} (increase optomechanical coupling). However, for rail thicknesses larger than 190 nm (such as the 400 nm rail width, circled in blue in Fig. 6(a) and shown in Fig. 6(b)), there is significant decrease in confinement of the optical mode because the light can partially "spill around" the holes through the wide rails. The mechanical mode, in contrast, stays relatively confined. The net effect is that the optical energy is "wasted" on parts of the structure that do not have significant motion, and the optomechanical coupling is again decreased.

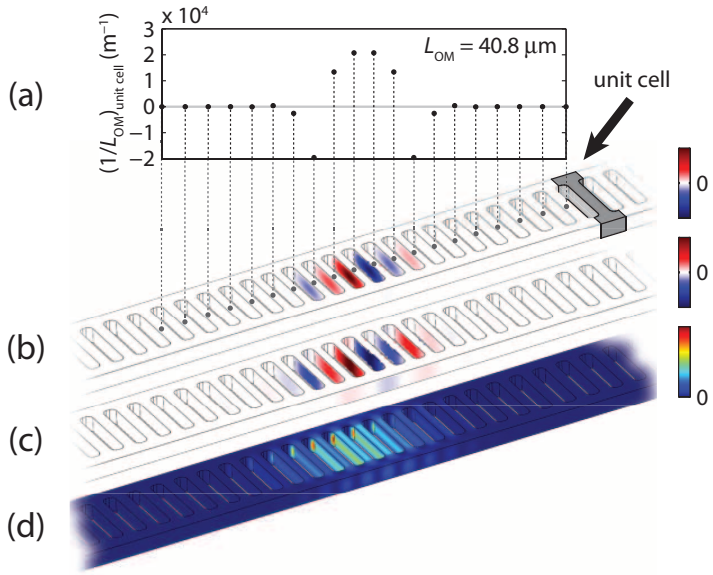

Fig. 7. For the fundamental pinch mode and the fundamental optical mode in the nominal structure, **(a)** FEM simulation of individual unit cell contributions to the total optomechanical coupling, **(b)** surface plot of the optomechanical coupling density, **(c)** surface plot of the normal displacement profile (Equation 10), **(d)** surface plot of the electromagnetic energy functional (Equation 11).

Just as Q_{m} is affected by hybridization of the breathing mode with propagating and body

#115150 - $15.00 USD Received 3 Aug 2009; revised 14 Sep 2009; accepted 22 Sep 2009; published 20 Oct 2009

modes, L_{OM} is affected by hybridization as $\mathbf{q}(\mathbf{r})$ is modified by the coupling to waveguide or body modes. This is responsible for the oscillations in L_{OM} seen in Fig. 6(a). The impact of coupling to the nanobeam body modes can be clearly seen in Fig. 6(c), where the breathing mode in a structure with a rail thickness of 230 nm has been plotted for two different beam lengths (number of total holes). For 47 total holes (circled in orange in Fig. 6a)), the breathing mode shape is altered significantly by the hybridization, causing the L_{OM} to deviate from the trend indicated by the red line in Fig. 6a). Shortening the structure by 2 holes (one on each side) decreases the coupling of the breathing mode to the propagating mode, returning L_{OM} to the trend line.

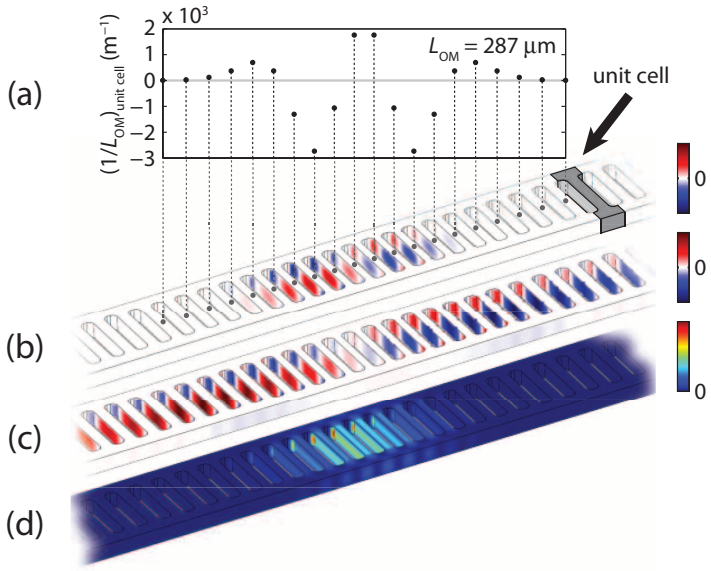

Fig. 8. For the accordion mode and the fundamental optical mode in the nominal structure, **(a)** FEM simulation of individual unit cell contributions to the total optomechanical coupling, **(b)** surface plot of the optomechanical coupling density, **(c)** surface plot of the normal displacement profile (Equation 10), **(d)** surface plot of the electromagnetic energy functional (Equation 11).

The pinch mode is a localized, in-plane differential acoustic vibration. Each neighboring crossbar vibrates 180 degrees out of phase with its nearest neighbors, since the pinch mode is drawn from a band edge at the *X* point. So although the optomechanical coupling contribution from each half of the structure (with respect to the *y*-*z* plane) is equal, such that the two halves add constructively to L_{OM}^{-1}, on either side of the *y*-*z* plane, contributions to L_{OM}^{-1} from neighboring crossbars tend to cancel. This puts a premium on mechanical localization, as a more localized pinch mode has a larger difference (and thus a reduced cancellation) between neighboring crossbars. Although the envelope of the pinch mode's displacement profile is gaussian, each crossbar is very rigid, so the displacement of the compression and tension faces of each crossbar is essentially identical (but opposite). The gaussian envelope only serves to change the relative vibration amplitudes of neighboring crossbars. The optomechanical coupling contribution from each crossbar would be approximately *zero* if it weren't for the rapid variation of the optical mode's envelope, and the contribution of each crossbar to L_{OM}^{-1} depends primarily on the difference in the optical energy density across the width of the beam. This would then lead one to believe that tighter localization, both optically and mechanically, would produce

#115150 - $15.00 USD Received 3 Aug 2009; revised 14 Sep 2009; accepted 22 Sep 2009; published 20 Oct 2009

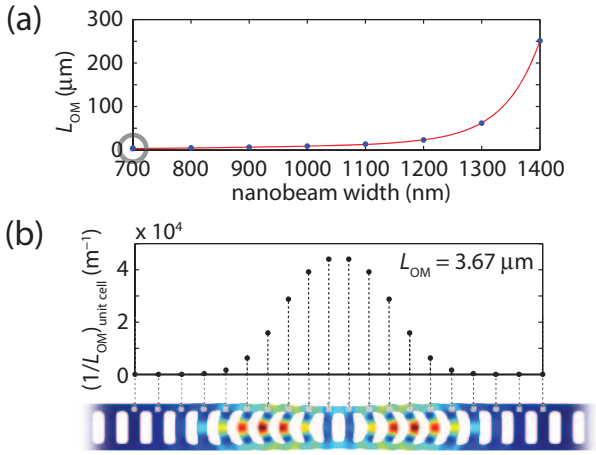

Fig. 9. For the accordion mode with the fundamental optical mode, **(a)**, the effective length as a function of total beam width, **(b)**, individual unit cell contributions to the total optomechanical coupling for a structure with a beam width of 700 nm (circled in (a)), mode frequency of 3.97 GHz and effective motional mass of 334 fg, with accompanying mechanical mode plot. The narrower mechanical mode (represented here by the deformation of the structure with color indicating relative strain) envelope results in drastically different optomechanical coupling contributions compared to Fig. 8.

better optomechanical coupling for this structure. Indeed, although the L_{OM} of the pinch mode in the structure shown is quite modest (≈ 41 μm), L_{OM} can be reduced to less than 3 μm by more tightly confining the optical and mechanical modes by reducing the number of holes involved in the defect region. There is, however, a loss of optical Q associated with the increased confinement due to the larger optical momentum components associated with tighter spatial localization. However, the structure as shown has a radiation-limited optical Q greater than 10 million; so it can be quite reasonable to trade optical Q for higher optomechanical coupling.

The last type of mechanical mode to be considered is the accordion mode (Fig. 8). The relatively poor L_{OM} for the accordion mode in the nominal structure is partly due to the fact that the rails recoil against the motion of the cross bar, producing opposing optomechanical contributions within each unit cell. In addition, the coupling of the broad first order Hermite-Gauss envelope of the mechanical mode with the narrower optical mode induces cancellations in the optomechanical coupling contributions at the inflection points of the mechanical mode envelope.

As discussed above, the accordion mode has a large effective mechanical bandgap. The dramatically increased Q_{m} that results makes it worthwhile to investigate whether the structure can be modified to produce smaller L_{OM}. By reducing the width of the nanobeam, it can be seen from Fig. 9(a) that the coupling is dramatically improved by almost two orders of magnitude when the width of the structure is reduced. As shown in Fig. 9(b), for a beam width of 700 nm, the contributions within each unit cell no longer cancel, due to the comparatively narrower mechanical mode envelope, and the structure yields $L_{\mathrm{OM}} = 3.67$ μm. In addition, simulations of the Q_{m} show that the effective bandgap for this narrower structure is approximately 2 GHz, yielding an extremely large Q_{m} for a given number of holes in the mirror section ($Q_{\mathrm{m}} \approx 10^8$ for 35 total holes). It should be noted that the frequency of the accordion mode of the narrower structure is approximately 4 GHz, up from 1.5 GHz in the wider structure.

#115150 - $15.00 USD Received 3 Aug 2009; revised 14 Sep 2009; accepted 22 Sep 2009; published 20 Oct 2009

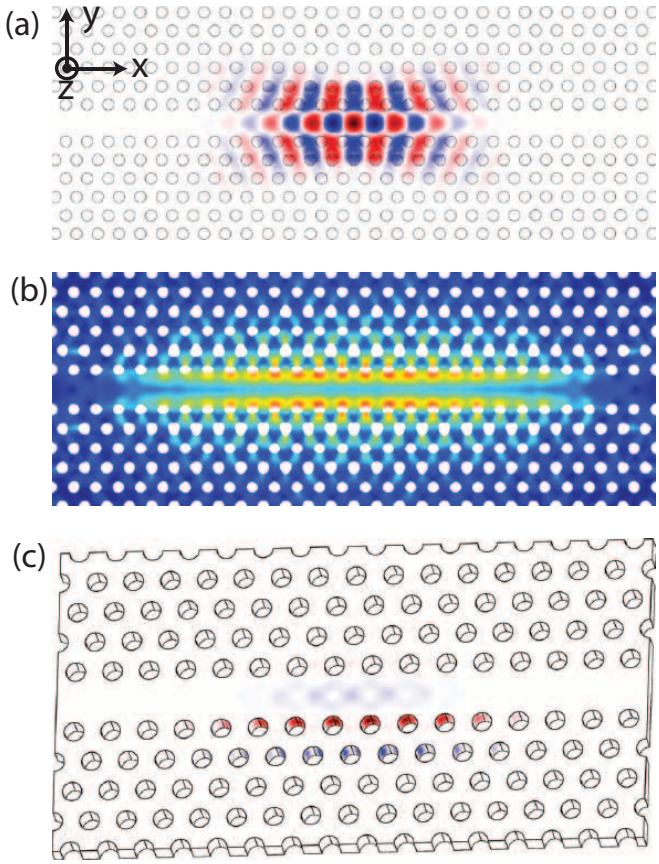

Fig. 10. **(a)** Fundamental optical mode of the double-heterostructrure OMC (geometry identical to that described in Ref. [35]), with $\lambda_0 \approx 1.5\ \mu$m, $Q_{\rm rad} \approx 2.7 \times 10^7$, and $V_{\rm eff} = 1.2\ (\lambda_0/n)^3$. **(b)** Breathing mechanical mode of the double-heterostructure OMC, with $\nu_{\rm m} = 9.3$ GHz, and $m_{\rm eff} = 322$ femtograms. **(c)** Optomechanical coupling integrand plotted on the double-heterostructure OMC system's surface; the structure has an $L_{\rm OM} = 1.75\ \mu$m for the optical-mechanical mode-pair from 10(a) and 10(b).

6. Optomechanical coupling in two-dimensional optomechanical crystals

As a final example of how these methods can be used to understand the optomechanical coupling in periodic structures with complex mechanical and electric field profiles, we model a double heterostructure hexagonal photonic crystal slab resonator. This is a well-known optical system, which has been found to have radiation-limited quality factors in excess of twenty million, with experimental demonstrations exceeding quality factors of two million[35]. The system consists of a hexagonal lattice of air holes in a silicon slab, with a single row of holes removed to create a waveguide mode within the optical stop band (the defect pulls the waveguide mode from the conduction band); in addition, the spacing in the direction of the waveguide is abruptly decreased twice to provide longitudinal confinement. This structure is essentially equivalent to the nanobeam structure, with the optical and mechanical modes guided by Bragg reflection in the lateral direction, as opposed to total internal reflection and hard boundaries in the nanobeam. With this in mind, we expect very similar optical and mechanical modes

#115150 - $15.00 USD Received 3 Aug 2009; revised 14 Sep 2009; accepted 22 Sep 2009; published 20 Oct 2009

wherever lateral propagation out of the waveguide is prohibited by Bragg reflection.

The fundamental optical cavity mode of the structure (the geometry is identical to that described in Ref. [35]) has been reproduced by FEM simulation and shown in Fig. 10(a). The structure also exhibits a lateral mechanical breathing mode at 9.3 GHz with a motional mass of 300 femtograms, modulating the width of the waveguide in a way that is analogous to the mechanical breathing mode of the nanobeam. The breathing mode displacement profile is shown in Fig. 10(b).

Figure 10(c) shows the integrand of the optomechanical coupling integrand (Eq. (8)) between the optical mode and the mechanical breathing mode plotted on the surface of the structure. The structure is shown slightly tilted to allow the insides of the holes to be seen, which give the dominant contributions to the optomechanical coupling. It is interesting to note that the coupling comes almost entirely from the movement of a small part of the interior of the holes (i.e., the region of the inner sidewall of the hole, closest to the center defect region); this can be seen by comparing the top half of the structure to the bottom half (since the integrand is symmetric about the *x*-*z* plane). Since each row of holes provides an opposite contribution to its neighbors, it is necessary to have a rapidly decaying optical envelope to achieve small L_{OM}, which is the case for the optical mode shown here. There is also a very small, opposing contribution from the center waveguide due to buckling/extrusion of the structure as the width is modulated. Just as in the case of the nanobeam, this optical-mechanical mode-pair has a very strong dispersive coupling, and evaluating the integral yields an effective length of only 1.75 μm.

Optically, the structure has a complete photonic bandgap for in-plane propagation, but, with a hole size to lattice constant ratio of $r/\Lambda = 0.26$, there is no corresponding in-plane mechanical bandgap. This makes the structure susceptible to mechanical loss mechanisms similar to those of the nanobeam. However, the two-dimensional hexagonal lattice, as well as other two dimensional Bravais lattices, can have simultaneous optical and mechanical bandgaps[62, 63], allowing the possibility of highly localized, low-loss optical-mechanical mode-pairs with very small effective lengths and motional masses.

Acknowledgements

This work was funded through the NSF under EMT grant no. 0622246, MRSEC grant no. DMR-0520565, and CIAN grant no. EEC-0812072 through University of Arizona.

#115150 - $15.00 USD Received 3 Aug 2009; revised 14 Sep 2009; accepted 22 Sep 2009; published 20 Oct 2009